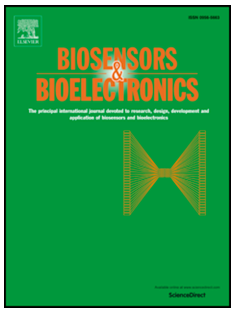

CRISPR/Cas9 cleavage triggered ESDR for circulating tumor DNA detection based on a 3D graphene/AuPtPd nanoflower biosensor

Mei Chen, Dongming Wu, Shihua Tu, Chaoyin Yang, DeJie Chen, Ying Xu

PII: S0956-5663(20)30807-1

DOI: https://doi.org/10.1016/j.bios.2020.112821

Reference: BIOS 112821

To appear in: *Biosensors and Bioelectronics*

Received Date: 25 September 2020

Revised Date: 10 November 2020

Accepted Date: 12 November 2020

Please cite this article as: Chen, M., Wu, D., Tu, S., Yang, C., Chen, D., Xu, Y., CRISPR/Cas9 cleavage triggered ESDR for circulating tumor DNA detection based on a 3D graphene/AuPtPd nanoflower biosensor, *Biosensors and Bioelectronics* (2020), doi: https://doi.org/10.1016/j.bios.2020.112821.

CRediT Author Statement

Ying Xu: Conceptualization, Methodology, Software. **Dongming Wu**: Data curation, Writing-Original draft preparation. **Shihua Tu**: Visualization, Investigation. **Chaoyin Yang***:* Supervision. **DeJie Chen**: Software, Validation. **Mei Chen:** Writing-Reviewing and Editing.

Biosensors and Bioelectronics *– Research Article*

CRISPR/Cas9 cleavage triggered ESDR for circulating tumor DNA detection based on a 3D graphene/AuPtPd nanoflower biosensor

Mei Chen [a], Dongming Wu [a], Shihua Tu [b], Chaoyin Yang [b], DeJie Chen [b], Ying Xu [a*]

[a] Clinical Laboratory, Clinical Medical College and The First Affiliated Hospital of Chengdu Medical College, Chengdu, Sichuan 610500, P.R. China

[b] School of Bioscience and Technology, Chengdu Medical College, Chengdu, Sichuan 610500, P.R. China

* **Corresponding Authors:**

Ying Xu. Tel.: +862883016721; Fax: +862862739582.
E-mail address: yingxu825@126.com (Y. Xu).

ABSTRACT

Circulating tumor DNA (ctDNA) plays an important role in the early diagnosis and prognosis of several cancers and is a credible biomarker for predicting the response to therapy. Additionally, the fact that the strategy used to detect ctDNA is non-invasive also adds to the advantages of using ctDNA for predicting disease diagnosis and prognosis. However, low abundance in peripheral blood and the high background of wild-type DNA impair the precise and specific measurement of ctDNA. In this study, we developed a novel 3D GR/AuPtPd nanoflower sensing platform based on CRISPR/Cas9 cleavage-triggered entropy-driven strand displacement reaction (ESDR) for the effective detection of ctDNA. Low levels of ctDNA could be detected using this method as the ESDR amplification does require complicated operation procedures and stringent reaction conditions. By combining the advantages of the site-specific cleavage by "gene magic scissors," Cas9/sgRNA, with those of the rapid amplification kinetics of entropy-driven strand displacement, our method resulted in amplification efficiency as well as high specificity for discriminating single-nucleotide mismatches. The 3D GR/AuPtPd nanoflower-based electrochemical biosensor displayed high specificity and worthy performance in assays with human serum. Therefore, this pioneered method provides a new paradigm for efficient ctDNA detection and shows great potential for use in clinical and diagnostic applications.

Keywords:

CRISPR; ESDR; Trimetallic nanoflower; Circulating tumor DNA; Biosensor

1. Introduction

Non-invasive “liquid biopsy,” involving the detection of circulating tumor DNA (ctDNA), plays an important role in the early diagnosis and prognosis of several cancers (Chi 2016; Santarpia et al. 2018). The presence of ctDNA in peripheral blood implies that the tumor is progressing toward malignancy (Lim et al. 2018). DNA enzyme inhibitors in the blood of tumor patients can inhibit the degradation of ctDNA in the plasma and lead to the accumulation of ctDNA in peripheral blood. As effective tumor-related biomarkers, ctDNAs are double-stranded circulating DNA fragments that carry tumor-specific sequence mutations and are present in the cell-free fraction of the blood (Wan et al. 2017).

Blood contains low levels of ctDNA (only 1% of cell-free DNA)(Kaiser 2010); thus, its clinical quantitative detection is mainly based on polymerase chain reaction (PCR) techniques such as reverse transcription quantitative PCR (RT-qPCR), asymmetric PCR, and droplet digital PCR (ddPCR) (Kiselinova et al. 2014; Plagnol et al. 2018). However, the requirement for a thermal cycler and cumbersome operational steps makes this approach difficult to implement in areas with limited resources and as a point-of-care test. To date, various enzyme-assisted signal amplification methods, including rolling circle amplification (RCA) (Wang et al. 2014), helicase-dependent amplification (HDA) (Barreda-Garcia et al. 2015), and exponential amplification reaction (EXPAR) (Li et al. 2016), have been employed to overcome the limitations of standard PCR methods. The use of enzymes in these strategies significantly enhances the detection sensitivity, however, it may lead to non-specific and false-positive signals. Moreover, enzymes are expensive and controlling reaction conditions to ensure optimal enzymatic activity is challenging.

Entropy-driven strand displacement reaction (ESDR), a promising enzyme-free reaction, employs several single-stranded DNA (ssDNA) molecules that are driven forward thermodynamically by the entropic gain of liberated molecules (Chen et al. 2016; Qian and Winfree 2011). ESDR has prominent advantages, which include its

simple design, speed, stability, and low non-specific background signals compared to other signal amplification strategies (He et al. 2020). To date, ESDR has been used for the detection of nucleic acids, and it has been used in molecular circuits (Peng et al. 2017) and DNA nanoswitches (Liu et al. 2018; Zhang et al. 2020). However, ESDR must be triggered by an accurate primer chain, a key factor in this amplification method, which may seriously affect the practical application of ESDR.

Recently, CRISPR/Cas9 (clustered regularly interspaced short palindromic repeats/CRISPR-associated nuclease 9) has emerged as a novel tool for accurate nucleic acid detection owing to its high efficiency and speed (Chen et al. 2017a; Nishimasu et al. 2018). Cas9 serves as a programmable nucleic acid “nicking” tool for site-specific cleavage of target ssDNA sequences, and has the advantages of simple composition and high cutting efficiency (Haapaniemi et al. 2018; Hu et al. 2018). Under the guidance of sgRNA, the Cas9 protein locate to the Protospacer Adjacent Motif (PAM), and cleavage the DNA chain near the PAM site. Thusa long target DNA sequence can be selectively cleaved by Cas9/single guide RNA (sgRNA) and provide a precise primer target chain for ESDR, ensuring specificity of signal amplification.

The use of biosensors is promising for the early detection and diagnosis of nucleic acid. To improve the sensitivity of electrochemical DNA biosensors, nanomaterials such as mesoporous silica, metallic nanomaterials (Lu et al. 2018; Zhao et al. 2019), and graphene have been used in recent years (Chen et al. 2017b; Vermisoglou et al. 2020). The self-assembled three-dimensional structural of graphene (3D GR) has been widely used in electronic devices, supercapacitors, and is a promising electrocatalyst has been explored for biosensors(Chen et al. 2018; Feng et al. 2015). Owing to the low charge transfer resistance and abundant active sites of the 3D GR lamellar structure, its composite with nanomaterials made of noble metals, such as gold (Au)(Zeng et al. 2018), silver (Ag)(Yang et al. 2018), palladium (Pd)(Yan et al. 2019), or platinum (Pt)(Salamifar and Lai 2014), shows better performance when coupled with electrochemical biosensors. Trimetallic nanomaterials consisting of different metal elements generally possess several

characteristics that are better than those of single-metal and bimetallic constituents, such as higher electrocatalytic activity and chemical stability (Dou et al. 2018; Yan et al. 2018). Moreover, due to their highly branched and flower-like structures, they exhibit an improved catalytic activity.

In this study, a CRISPR/Cas9 triggered ESDR system based on the 3D GR/AuPtPd nanoflower biosensor was successfully constructed to detect the mutated epidermal growth factor receptor (EGFR) ctDNA for the first time. The guiding principle of the technique has been elaborated in Figure 1. The “nicking” tool of the Cas9/sgRNA complex rapidly recognized and cleaved the target in the original DNA sequence. This novel approach provided the precise primer target chain required for the subsequent ESDR step. Next, the target DNA triggered the ESDR that created a triplicate DNA substrate probe, formed by the T1, R1, and S1 chains. The trigger resulted in the release of the initial target sequence, which acted as a promoter for the next cycle, thereby providing highly superimposed signal variations. Finally, the 3D GR/AuPtPd hybridized nanoflowers were confirmed to be an excellent electrochemical sensing platform, which significantly enhanced the sensitivity for ctDNA detection using the CRISPR/Cas9-triggered ESDR. This innovative strategy can serve as a versatile DNA detection method for bioanalysis and clinical diagnostics.

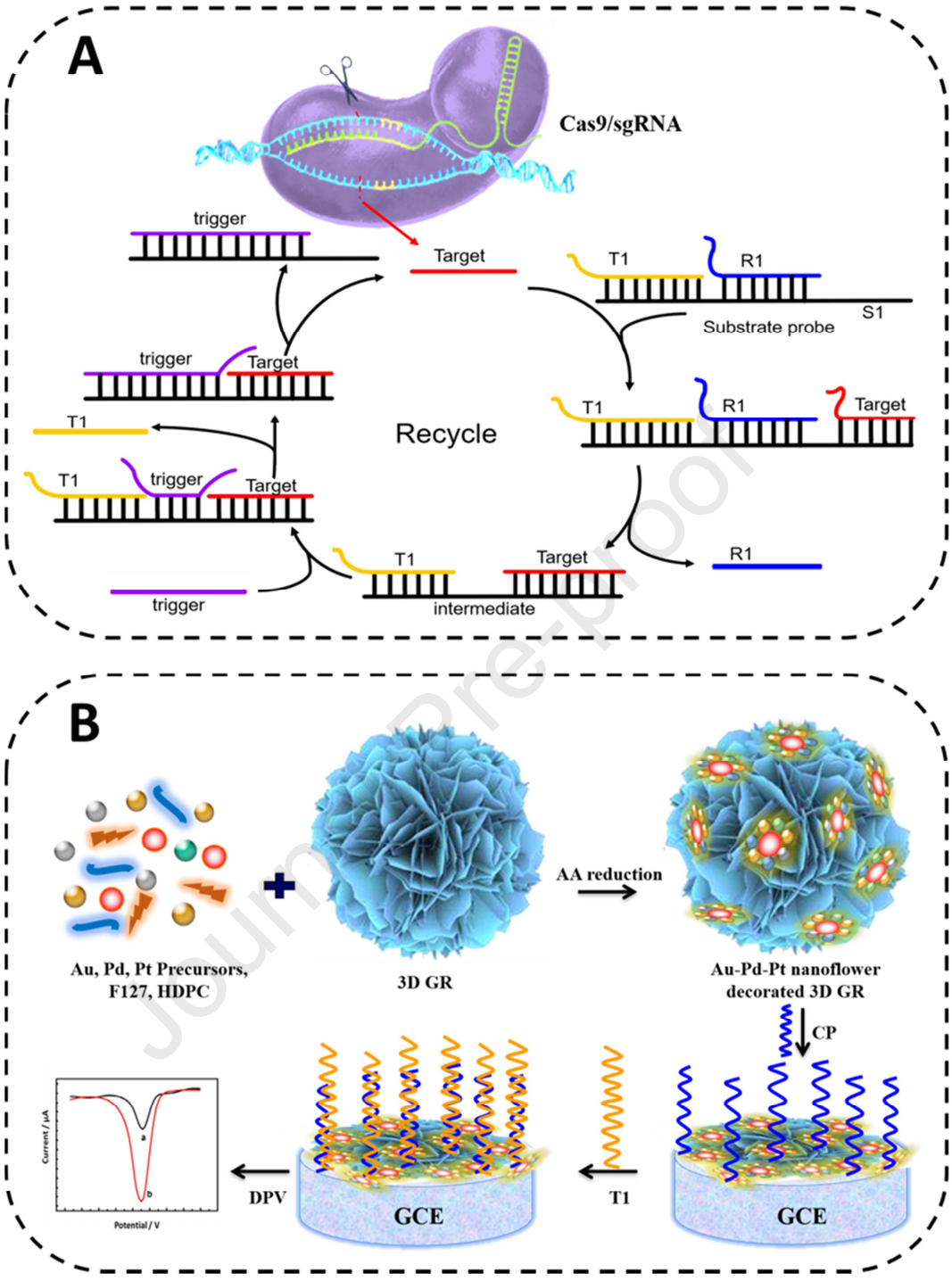

Figure 1. Schematic of the principle of the CRISPR/Cas9-triggered ESDR based on a 3D GR/AuPtPd nanoflower biosensor. (HDPC, hexadecylpyridinium chloride monohydrate; AA, L-ascorbic acid; CP, Capture probe; GCE, glassy carbon electrode).

2. Experimental section

2.1. Apparatus and Materials

Morphological characterization of the nanomaterials was performed using a Nova 400 scanning electron microscope (SEM) (FEI, Hillsboro, ORE, USA) and JEM-2100 transmission electron microscope (TEM) (Hitachi, Japan). X-ray photoelectron spectroscopy (XPS) was characterized using an ESCALAB 250 spectrometer (Thermo Electron, U.K.). The specific surface areas of the nanomaterials were determined by a surface area analyzer (NOVA 2000, Quantachrome) using physical adsorption/desorption of N_2 at the liquid-N_2 temperature. PCR was performed using a gradient PCR cycler (Eppendorf, Hamburg, Germany), and electrophoresis gel images were visualized using a UV transilluminator (Bio-Rad, Hercules, USA). Electrochemical measurements were performed using a CHI600E workstation (CH Instruments, Austin, TX, USA).

Cas9 protein, T7 RNA polymerase, and reaction buffer were purchased from Genscript (Piscataway, NJ. USA). Pluronic F127 (Mw = 12,600), hexadecylpyridinium chloride monohydrate (HDPC, 98%), graphene oxide powder, $HAuCl_4$ (99%), Tris-HCl, 6-mercapto-1-hexanol (MCH), Na_2PdCl_4 (98%), L-ascorbic acid (AA), and K_2PtCl_4 (99%) were purchased from Sigma-Aldrich (St. Louis, MO, USA). The detection sequence selected the 15del mutated in Exon 19 of EGFR. All oligonucleotides were synthesized and purified by Tsingke BioTech (Tsingke, China), and the sequences are listed in Table S1. All other reagents were purchased from Chengdu Kelong Chemical (Chendu, China).

2.2 Synthesis and purification of sgRNA

Fill-in PCR was performed according to the following protocol: initial denaturation at 95 °C for 2 min; 35 cycles of 95 °C for 15 s, 65 °C for 30 s, and 72 °C for 1 min; and a final extension at 72 °C for 2 min. The two PCR products were used as templates for T7 RNA polymerase-mediated transcription. sgRNAs were

transcribed using the HiScribe T7 Quick High Yield RNA Synthesis Kit (Tiangen Biotech, Sichuan, China). The transcribed sgRNAs were purified using the RNAclean Kit (Sangon Biotech, Shanghai, China). sgRNAs were stored at −80 °C for further use.

2.3 In vitro Cas9/ sgRNA cleavage assay

First, Cas9 nuclease (1 μg) and sgRNA (200 ng) were added to a reaction mixture (20 μL) containing reaction buffer (10X, RNase-free H_2O), and preincubated at 25 °C for 5 min. Second, different concentrations of target dsDNA substrate were added into the mixed solution and incubated at 37 °C for 60 min. Third, the final reaction was terminated after heating at 70 °C for 10 min, and agarose gel electrophoresis was performed to visualize the cleavage products.

2.4 ESDR

T1 (3 μM) and R1 (3 μM) were first incubated with the S1 chain (3 μM) in a hybridization solution at 90 °C for 10 min, and after cooling to 25 °C, the substrate probe was obtained. Next, the trigger (2 μM) was added to the reaction solution. Subsequently, the target obtained from Cas9 cleavage products was added and incubated to facilitate the strand displacement cycle reaction for attaining signal amplification.

2.5 Synthesis of 3D GR/AuPtPd nanoflowers

The 3D GR/AuPtPd nanoflowers were synthesized using a modified one-step wet-chemical method(Huang et al. 2013). First, Pluronic F127 (4.3 mg) and HDPC (0.35 mg) were dissolved in an aqueous solution (2.5 mL). Second, $HAuCl_4$ (10 mM, 30 μL), K_2PtCl_4 (10 mM, 120 μL), and Na_2PdCl_4 (10 mM, 120 μL) were sequentially

added to the aqueous solution and gently stirred so that they combined effectively. Then, 3D GR (400 μL, 2 mg mL^{-1}) was added and sonicated for 30 min. Next, AA (30 mM, 350 μL) was added with continuous stirring for 1 h. The resulting solution was centrifuged and cleaned with double-distilled water to obtain the 3D GR/AuPtPd nanoflowers.

2.6 Biosensor fabrication and electrochemical detection

First, the surface of the glassy carbon electrode (GCE) was cleaned and coated with 5 μL of 3D GR/AuPtPd(2 mg mL^{-1}), followed by the addition of 5 μL of the capture probe (CP) (0.01 μM) and incubated for 30 min at 30 °C to immobilize 5′-thiolated CP. Cyclic voltammetry (CV) was performed with cycling at a potential ranging from −0.2 to +0.6 V at a scan rate of 100 mV s^{-1}. Square wave voltammograms (SWVs) were recorded with 0.9 V scan increment and 3 V amplitude. Electrochemical impedance spectral (EIS) investigation was performed over a frequency range of 10^{-1} to 10^{5} Hz in $[Fe(CN)_6]^{3-/4-}$ (3 mM) containing KCl (0.1 M). Next, 10 μL of the Cas9-ESDR solution was dropped onto the CP/3D GR/AuPtPd /GCE for 60 min at 25 °C and terminated with a three-step washing step with buffer. Lastly, differential pulse voltammetry (DPV) was performed at −0.4 to +0.2 V at a sweeping rate of 100 mV s^{-1} to test the electrochemical response.

3. Results and discussion

3.1 Feasibility analysis of the CRISPR/Cas9 system

Sodium dodecyl sulfate-polyacrylamide gel electrophoresis (SDS-PAGE) was employed to validate the expression of Cas9 protein. As shown in Figure 2A, the visible 160.5 kDa protein band of purified Cas9 (Line 5) was consistent with the expected molecular weight. The synthesized sgRNA was visualized on a 2% agarose

gel (Fig. 2B), which met the requirements of subsequent cleavage experiments. Subsequently, the dsDNA substrate was incubated with the Cas9/sgRNA mixture and the cleavage products were detected (Fig. 2C). The position of the probe revealed that the large fragment was approximately 200 bp in size and the smaller fragment was 150 bp in size. The obtained bands in the electrophoretogram were consistent with the predicted length, indicating that the designed Cas9/sgRNA precisely performed the intended cleavage *in vitro*.

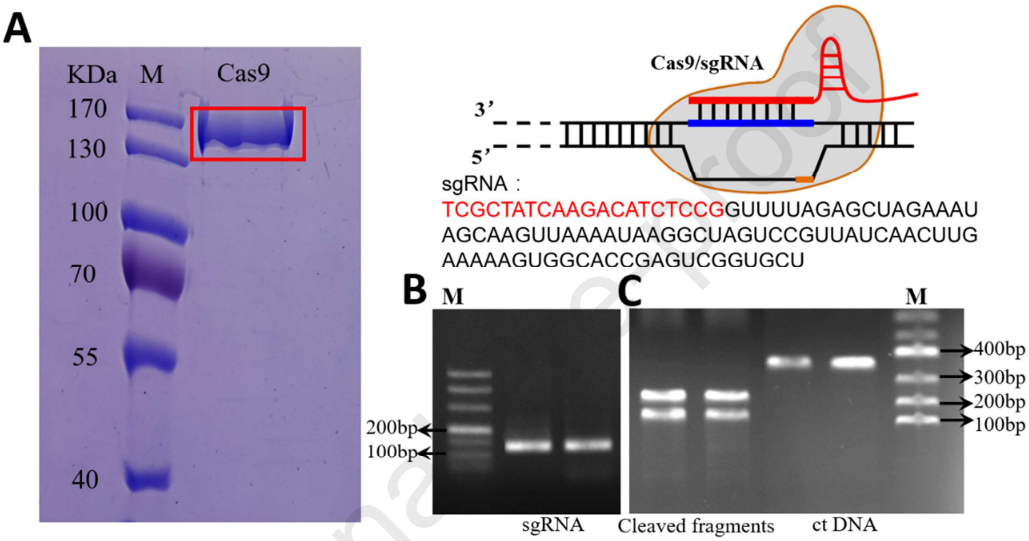

Figure 2. (A) SDS-PAGE analysis of Cas9 proteins. M: protein marker, Gel electrophoresis of the (B) synthesized sgRNA and (C) DNA samples after Cas9/sgRNA cleavage.

3.2 Characterization of the 3D GR/AuPtPd nanoflowers

The morphology of 3D GR/AuPtPd was studied using SEM and TEM. 3D GR looked like a hydrangea with several thin lamellar structures (Fig. 3A), indicating the presence of a three-dimensional structure with a large specific surface area. The micellar templates of Pluronic F127 and HDPC may have contributed to the formation of branched hybridized trimetallic nanoflowers. During this process, a part of the Au precursor is first reduced as the initial seed on the 3D GR substrate owing to the more positive standard reduction potential of Au ions; then, the Au, Pt, and Pd sources

rapidly nucleate, resulting in numerous aggregated trimetallic nanostructures uniformly distributed on the surface of the 3D GR nanosheets. Compared with the original 3D GR nanosheets (inset in Fig. 3B), the AuPtPd are well separated and uniformly dispersed on the 3D GR surface (Fig. 3B). TEM characterization further confirmed the details of the 3D GR/AuPtPd complexes. As shown in Fig. 3C–E, the size of the AuPtPd trimetallic nanohybrids, which had a highly branched nanoflower structure, was approximately 20–40 nm. The N_2 adsorption-desorption isotherms are given in Figure S1. The specific surface area of the AuPtPd, 3D GR and 3D GR/AuPtPd calculated using the multipoint Brunauer–Emmett–Teller (BET) method is 148.6 m^2 g^{-1}, 218.5 m^2 g^{-1} and 397.8 m^2 g^{-1}, respectively. This indicates the fabrication of AuPtPd onto the 3D GR nanosheets could increase their specific surface area and facilitate electron transfer due to the abundant trimetallic branches. Energy dispersive spectroscopy (EDS) profile (Fig. 3F) and elemental mapping image (Fig. 3G) confirmed that the nanoflowers were mainly composed of C, Au, Pt, and Pd, as expected. XPS was taken to analyze the chemical composition and surface atomic state of the 3D GR/AuPtPd further. The peaks are assigned to the binding energies of Pt4f, Au4f, C1s, Pd3d, and O1s, respectively (Fig. S2). All results confirmed that AuPtPd were successfully anchored on the 3D GR nanosheets.

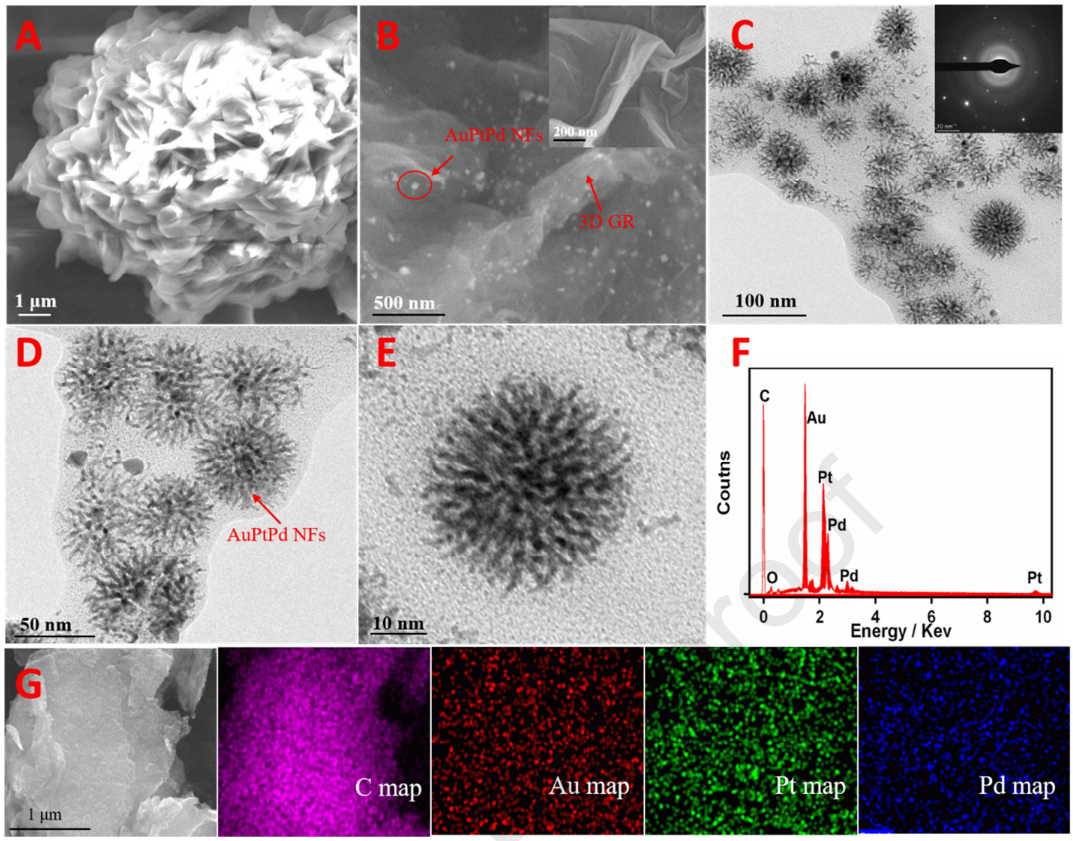

Figure 3. (A) SEM images of the 3D GR nanosheets and (B) AuPtPd nanoflower structures. (C, D) TEM and (E) high-resolution TEM images of the 3D GR/AuPtPd. (F) SEM-EDS profile and (G) EDS elemental mapping image of 3D GR/AuPtPd.

3.3 Electrochemical characterization of the biosensor

When 3D GR were modified on the surface of the GCE (curve b), the CV peak current was substantially higher than that for bare GCE (curve a), indicating that 3D GR served as an ideal electrically conductive material for the acceleration of the electron transfer rate of $[Fe(CN)_6]^{3-/4-}$ (Fig. 4A). The 3D GR/AuPtPd nanoflowers were assembled on the GCE, and the peak current increased significantly (curve c) owing to the synergistic enhancement of the catalytic activity driven by the trimetal hybrid nanoflowers and 3D GR nanosheets complexes. The CV current decreased (curve d) once the SH-modified captured probes were immobilized on the surface of the 3D GR/AuPtPd nanoflowers. The redox peaks also decreased after the MCH was

immobilized, because it prevented further electron transfer (curve e). The peak current further decreased (curve f) after the addition of the Cas9/ESDR products due to a negative charge enhancement triggered by the hybridization reaction.

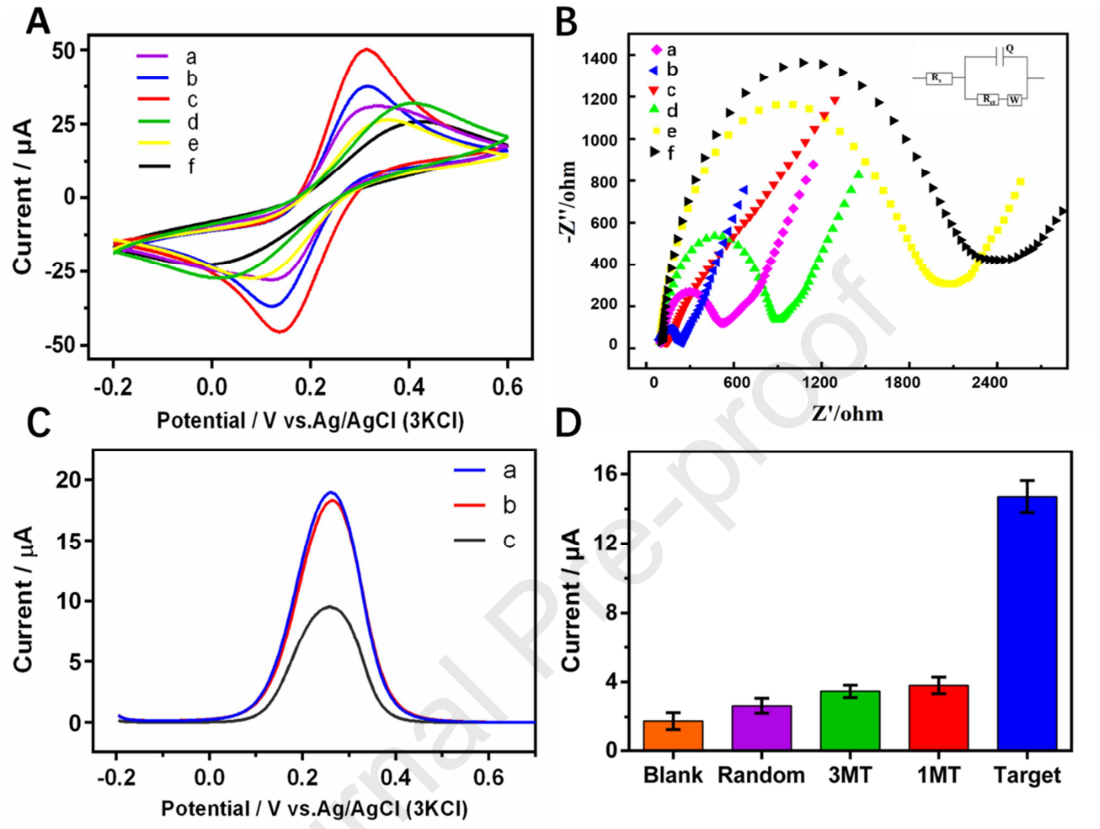

Figure 4. (A) CV response of different modified electrodes. (B) EIS characteristics of different modified electrodes in Fe $(CN)_6^{3-/4-}$ (1 mM) containing KCl (0.1 M) solution. (C) Feasibility analysis of the CRISPR/Cas9-triggered ESDR method. (D) Specificity of the biosensor.

EIS is an effective tool to verify the electron transfer resistance (Ret) in biosensor dynamic modification processes. As depicted in Fig. 4B, subsequent to the formation of highly branched nanoflower-like structures, a considerably lower Ret was observed for 3D GR/AuPtPd (curve c) compared with that for 3D GR (curve b), implying that trimetal nanoflowers facilitate a faster interfacial charge transfer and play an important role in accelerating the transfer of electrons. The Ret increased after the immobilization of Cp (curve d), suggesting that SH-modified probes were successfully deposited on the surface of 3D GR/AuPtPd nanoflowers. An increase in

Ret was observed after addition of MCH (curve e), which was attributed to the inhibitory effect of MCH on electron permeation. After hybridization, an increase in Ret was further observed (curve f), implying that the nucleic acid molecule had hybridized and added a negative charge. These results confirmed that each step in the biosensor fabrication had been performed successfully.

3.4 Feasibility and specificity of the novel biosensor

To investigate the feasibility of this biosensor, the SWV responses of different electrodes were determined (Fig. 4C). No obvious change in peak current was observed when only the CP/3D GR/AuPtPd/GCE complex (curve a) or the trigger strand (curve b) were incubated with the substrate probes, indicating that ESDR did not occur in the absence of the target. However, the current signal decreased significantly (curve c) after the addition of the target cleaved by the Cas9/sgRNA system. Overall, the cascade of strand displacement amplification reaction and the consequent nucleic acid hybridization with the CP/3D GR/AuPtPd nanoflowers resulted in the modification of the electrode surface. The specificity of these changes suggests that ESDR must be initiated by a precise target chain. This approach could even discriminate single-nucleotide mismatches, thereby effectively avoiding non-specific amplification. This was possible as the target chains were only generated after precise cutting by the Cas9/sgRNA bound to specific DNA sequences. These results clearly indicated the feasibility of using Cas9/sgRNA coupled with ESDR in this 3D GR/AuPtPd nanoflower sensing system.

To explore the specificity of the method, equal concentrations of the target, mutant target (MT), and the non-complementary sequence (random) were detected (Fig. 4D). The current of complementary target was significantly greater than those of the single-base mismatched (1MT) and three-base mismatched mutant target (3MT). The current of random strand showed an even smaller current, nearly the same as that of the blank control. The proposed amplification method was found to be highly

selective for the intended target; therefore, this biosensor may be employed to detect dsDNA.

3.5 Sensitivity of the biosensor

We investigated the sensitivity of this new method by analyzing different concentrations of the target ssDNA using DPV measurements (Fig. 5A). The current responses were observed to increase with increasing target concentrations (from 0 pM to 3 nM). Figure 5B illustrates the dependence of the current response on the target DNA concentrations (ranging from 0.01 to 500 pM). The current response showed a linear dependency on the target concentration, in the range from 0.01 pM to 500 pM, with a correlation coefficient of 0.921 (inset in Fig. 5B). The linear regression equation was ΔI (μA) = 16.35 + 8.312 log C (M), and the limit of detection (LOD) at a signal/noise ratio of 3 was calculated to be 0.13 pM.

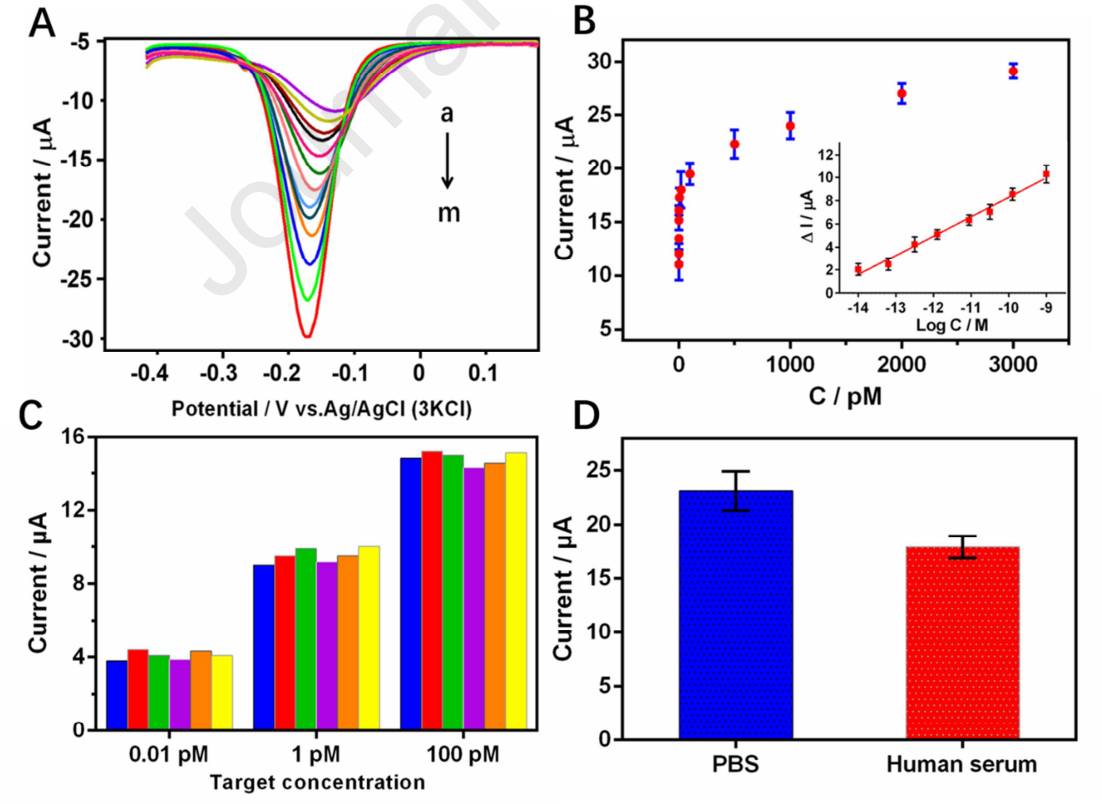

Figure 5. Analytical performance of the DNA biosensor. (A) DPV of the system with

328 an increasing concentration of target DNA (from a to m: 0, 0.01, 0.05, 0.2, 1, 2, 5, 20,
329 100, 500, 1000, 2000, and 3000 pM). (B) Linear relationship between the current
330 response suppression and target concentration. Inset: calibration curve of the DPV
331 current decrement versus the logarithm of the target concentration. (C)
332 Reproducibility of the electrochemical biosensor in different target concentrations. (D)
333 DPV peak current intensity for detecting *EGFR* (500 pM) in PBS and human serum.
334 The comparison between our biosensor and previously reported methods is
335 shown in Table S2. Overall, this novel strategy has several advantages over currently
336 available methods. First, owing to Cas9, it can serve as a powerful nucleic acid
337 "nicking" tool for site-specific cleavage of DNA sequences, avoiding primer-induced
338 non-specific triggering. Moreover, Cas9–ESDR detects specific long stretches of
339 DNA with high specificity, discriminates single-nucleotide mismatches with high
340 amplification efficiency compared with the standard ESDR. Second, the use of
341 nonenzymatic ESDR, with high superimposed signal variations, is an important new
342 step in the field of biosensors and provides a new detection tool that does not require
343 complicated operation procedures and stringent enzymatic reaction conditions. Third,
344 3D GR/AuPtPd nanoflowers were confirmed to be efficient, sensitive, and rapid
345 electrochemical sensing platforms owing to their three-dimensional flower-like
346 structure, which provides a large specific area and high electrochemical activity.
347
348 *3.6 Reproducibility, stability, and for clinical viability*
349
350 The reproducibility of the biosensor was evaluated by testing the reaction product
351 with varying concentrations (0.01, 1, and 100 pM) of the target (Fig. 5C). Each target
352 concentration was tested six times. The relative standard deviations for six
353 independent measurements were 7.9%, 6.2%, and 4.5%, for 0.01, 1, and 100 pM
354 targets, respectively. The stability of the assay was investigated using three
355 independent experiments. After adding a drop of PBS, the 3D GR/AuPtPd /GCE was
356 stored in air at 4 °C and it retained approximately 93.1% of its initial current response

after a storage period of two weeks. These results indicate that the biosensor possesses desired stability and reproducibility.

Table 1. Determination of ctDNA-EGFR in human serum samples (n = 4) using the proposed strategy

Samples	ctDNA-EGFR added (pM) *	Biosensing strategy detected (pM) *	Recovery (%)	Relative standard deviation (%)
1	2.0	2.23	111.5	6.33
2	20.0	18.35	91.75	4.17
3	50.0	49.16	98.32	3.65
4	100.0	106.28	106.28	9.26

*Each value is the mean of five replicate experiments.

The clinical viability of the proposed ctDNA biosensor was investigated in human serum samples containing mutation ctDNA-EGFR. As shown in Fig. 5D, the DPV signals of ctDNA in human serum showed a mild decline in contrast to that of PBS, which might be attributed to interference by complex media constituents. Under optimal experimental conditions, samples spiked with different concentrations of ctDNA (2 pM, 20 pM, 50 pM and 100 pM) were included (Table 1). Each sample was examined in three parallel tests. Satisfactory recovery values ranging from 91.75% to 111.5% with an RSD of 3.65%–9.26% were achieved, implying that this new strategy holds potential to monitor ctDNAs in complex biological samples.

4. Conclusions

In summary, we developed a CRISPR/Cas9 triggered ESDR system based on the 3D GR/AuPtPd nanoflower platform to detect circulating tumor DNAs. By combining the advantages of site-specific cleavage of Cas9/sgRNA and rapid amplification kinetics of ESDR, Cas9–ESDR showed remarkable performance, high specificity, and

signal enrichment. 3D GR/AuPtPd nanoflowers have a high specific surface area and serve an efficient sensing platform to analyze ctDNA. Benefiting from the high specificity and sensitivity due to the “Cas9-ESDR” and “3D GR/AuPtPd” effects, this powerful method has great potential for application in clinical molecular diagnosis, and provides a novel approach for “liquid biopsy. ”

Acknowledgments

The authors would like to acknowledge the financial support from “Foundation of Sichuan Science and Technology Agency (No. 2019YJ0365, 2019JY0589),” “The Central guide placeScience and Technology Development Project (No. 2020ZYD025),” “National Natural Science Foundation of Chengdu Medical College (No. CYCG18-04),” “Collaborative Innovation Center of Sichuan for Elderly Care and Health, Chengdu Medical College (No. 19Z07),” and “the National Natural Science Foundation of China (No. 31902398, 81601859).”

Declaration of interests

The authors declare that they have no known competing financial interests or personal relationships that could have influenced the work reported in this study.

References

Barreda-Garcia, S., Gonzalez-Alvarez, M.J., de-los-Santos-Alvarez, N., Palacios-Gutierrez, J.J., Miranda-Ordieres, A.J., Lobo-Castanon, M.J., 2015. Biosens.Bioelectron.Biosens Bioelectron. 68, 122-128.

Chen, H.G., Ren, W., Jia, J., Feng, J., Gao, Z.F., Li, N.B., Luo, H.Q., 2016. Biosens Bioelectron. 77, 40-45.

Chen, J.S., Dagdas, Y.S., Kleinstiver, B.P., Welch, M.M., Sousa, A.A., Harrington, L.B., Nature 550(7676), 407-+.

Chen, M., Hou, C.J., Huo, D.Q., Fa, H.B., Zhao, Y.N., Shen, C.H., 2017b. Sens. Actuators B Chem. 239, 421-429.

Chen, M., Wang, Y.Y., Su, H.L., Mao, L., Jiang, X.N., Zhang, T., Dai, X.Z., 2018. Sens. Actuators B Chem. 255, 2910-2918.
Chi, K.R., 2016. Nature. 532(7598), 269-271.
Dou, B.T., Yang, J.M., Yuan, R., Xiang, Y., 2018. Anal Chem. 90(9), 5945-5950.
Feng, X.M., Zhang, Y., Zhou, J.H., Li, Y., Chen, S.F., Zhang, L., Ma, Y.W., Wang, L.H., Yan, X.H., 2015. Nanoscale. 7(6), 2427-2432.
Haapaniemi, E., Botla, S., Persson, J., Schmierer, B., Taipale, J., 2018. Nature Medicine 24(7), 927-+.
He, Y.H., Cheng, L.J., Yang, Y.Y., Chen, P., Qiu, B., Guo, L.H., Wang, Y., Lin, Z.Y., Hong, G.L., 2020. Sens. Actuators B Chem. 320.
Hu, J.H., Miller, S.M., Geurts, M.H., Tang, W.X., Chen, L.W., Sun, N., Zeina, C.M., Gao, X., Rees, H.A., Lin, Z., Liu, D.R., 2018. Nature 556(7699), 57-59.
Huang, X.Q., Li, Y.J., Chen, Y., Zhou, E.B., Xu, Y.X., Zhou, H.L., Duan, X.F., Huang, Y., 2013. Angew Chem Int Edit 52(9), 2520-2524.
Kaiser, J., 2010. Science 327(5969), 1072-1074.
Kiselinova, M., Pasternak, A.O., De Spiegelaere, W., Vogelaers, D., Berkhout, B., Vandekerckhove, L., 2014. Plos One 9(1).
Li, J.L., Chen, Z.P., Xiang, Y., Zhou, L.L., Wang, T., Zhang, Z., Sun, K.X., Yin, D., Li, Y., Xie, G.M., 2016. Biosens.Bioelectron. 86, 75-82.
Lim, M., Kim, C.J., Sunkara, V., Kim, M.H., Cho, Y.K., 2018. Micromachines 9(3).
Liu, N., Xu, K., Liu, L.Q., Chen, X., Zou, Y.F., Xiao, X.J., 2018. Microchim Acta. 185(9).
Lu, H.J., Pan, J.B., Wang, Y.Z., Ji, S.Y., Zhao, W., Luo, X.L., Xu, J.J., Chen, H.Y., 2018. Anal Chem. 90(17), 10434-10441.
Nishimasu, H., Shi, X., Ishiguro, S., Gao, L.Y., Hirano, S., Okazaki, S., Noda, T., Abudayyeh, O.O., et al., 2018. Science 361(6408), 1259-1262.
Peng, P., Shi, L.L., Wang, H.H., Li, T., 2017. Nucleic Acids Res.45(2), 541-546.
Plagnol, V., Woodhouse, S., Howarth, K., Lensing, S., Smith, M., Epstein, M., C., et al., 2018. Plos One 13(3).
Qian, L., Winfree, E., 2011. Science 332(6034), 1196-1201.
Salamifar, S.E., Lai, R.Y., 2014. Anal Chem. 86(6), 2849-2852.
Santarpia, M., Liguori, A., D'Aveni, A., Karachaliou, N., Gonzalez-Cao, M., Daffina, M.G., Lazzari, C., Altavilla, G., Rosell, R., 2018. J Horac Dis.10, S882-S897.
Vermisoglou, E., Panacek, D., Jayaramulu, K., Pykal, M., Frebort, I., Kolar, M., Hajduch, M., Zboril, R., Otyepka, M., 2020. Biosens.Bioelectron.166.
Wan, J.C.M., Massie, C., Garcia-Corbacho, J., Mouliere, F., Brenton, J.D., Caldas, C., Pacey, S., Baird, R., Rosenfeld, N., 2017. Nat. Rev. Cancer 17(4), 223-238.
Wang, Q., Yang, C.Y., Xiang, Y., Yuan, R., Chai, Y.Q., 2014. Biosens.Bioelectron. 55, 266-271.
Yan, Q., Cao, L.L., Dong, H., Tan, Z.L., Liu, Q., Zhang, W., Zhao, P.P., Li, Y.Y., Liu, Y.Y., Dong, Y.H., 2019. Anal Chim Acta. 1069, 117-125.
Yan, Q., Yang, Y.Y., Tan, Z.L., Liu, Q., Liu, H., Wang, P., Chen, L., Zhang, D.P., Li, Y.Y., Biosens.Bioelectron.103, 151-157.
Yang, Y.Y., Yan, Q., Liu, Q., Li, Y.P., Liu, H., Wang, P., Chen, L., Zhang, D.P., Li, Y.Y., Dong, Y.H., 2018. Biosens. Bioelectron .99, 450-457.
Zeng, Y., Bao, J., Zhao, Y.N., Huo, D.Q., Chen, M., Yang, M., Fa, H.B., Hou, C.J., 2018. Talanta

178, 122-128.
Zhang, R.F., Li, S.S., Wang, J.F., Qu, X.N., Zhao, Y.H., Liu, S., Wang, Y., Huang, J.D., Yu, J.H., 2020. Sens. Actuators B Chem. 320.
Zhao, H., Liu, F., Lu, Y.X., Jin, L., Tan, S., Zhang, Y.P., Li, C.P., 2019. Sens. Actuators B Chem.285, 553-561.

463

Highlights

- An CRISPR/Cas9 triggered ESDR system is firstly manufactured for specific cleavage and has high amplification efficiency.
- 3D GR/AuPtPd nanoflower was confirmed to be an efficient, ultrasensitive, and rapid electrochemical sensing platform.
- The high specificity of Cas9–ESDR could discriminated a single-base mismatched sequence from the perfectly complementary one.
- This newly-developed three-dimensional biosensor was successfully used for detecting EGFR in human serum.

Declaration of interests

☒ The authors declare that they have no known competing financial interests or personal relationships that could have appeared to influence the work reported in this paper.

☐The authors declare the following financial interests/personal relationships which may be considered as potential competing interests: